ACS BIO & MED CHEM Au
AN OPEN ACCESS JOURNAL OF THE AMERICAN CHEMICAL SOCIETY

pubs.acs.org/biomedchemau

Article

Pre-Existing Oxidative Stress Creates a Docking-Ready Conformation of the SARS-CoV-2 Receptor-Binding Domain

Carl J. Fossum, Bethany F. Laatsch, Harrison R. Lowater, Alex W. Narkiewicz-Jodko, Leo Lonzarich, Sanchita Hati,* and Sudeep Bhattacharyya*

Cite This: https://doi.org/10.1021/acsbiomedchemau.1c00040

Read Online

ACCESS | Metrics & More | Article Recommendations | Supporting Information

ABSTRACT: The redox-dependent changes on the binding between the receptor-binding domain of the severe acute respiratory syndrome-coronavirus-2 spike protein and the peptidase domain of the human cell surface receptor angiotensin-converting enzyme II were investigated by performing molecular dynamics simulations. The reduced states of the protein partners were generated in silico by converting the disulfides to thiols. The role of redox transformation on the protein−protein binding affinity was assessed from the time-evolved structures after 200 ns simulations using electrostatic field calculations and implicit solvation. The present simulations revealed that the bending motion at the protein−protein interface is significantly altered when the disulfides are reduced to thiols. In the native complex, the presence of disulfide bonds preserves the structural complementarity of the protein partners and maintains the intrinsic conformational dynamics. Also, the study demonstrates that when already bound, the disulfide-to-thiol conversion of the receptor-binding domain has a limited impact on the binding of the spike protein to the receptor. However, if the reduction occurs before binding to the receptor, a spectacular conformational change of the receptor-binding domain occurs that fully impairs the binding. In other words, the formation of disulfide bonds, prevalent during oxidative stress, creates a conformation ready to bind to the receptor. Taken together, the present study demonstrates the role of pre-existing oxidative stress in elevating the binding affinity of the spike protein for the human receptor, offering future clues for alternate therapeutic possibilities.

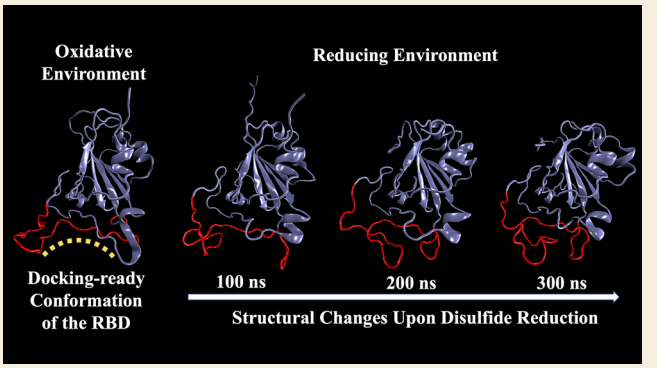

KEYWORDS: *COVID-19, oxidative stress, redox chemistry, spike protein binding, thiol−disulfide balance*

INTRODUCTION

With over 5 million people dead in almost two years, the coronavirus disease of 2019 (COVID-19) is still rapidly expanding to several parts of the world.[1] The largest public health crisis in modern world history, the disease and the subsequent global pandemic have disrupted the lives of billions with no end in sight. The disease is caused by the severe acute respiratory syndrome-coronavirus-2 (SARS-CoV-2), the seventh member of the *Coronaviridae* family. It is a positive-sense single-stranded RNA virus of the genus *Betacoronavirus*.[2,3] The coronavirus particles contain four main structural proteins: spike, membrane, envelope, and nucleocapsid. It is so named for the spike (S) proteins adorning the outer shell of the virus, giving coronaviruses the appearance of having "corona" or crown.[4,5] The S-protein has a receptor-binding domain (RBD) that interacts with the host cell receptor protein, angiotensin-converting enzyme-2 (ACE2), during the entry of the virus into a human cell.[6−8] SARS-CoV-2 is similar to two others of the family, namely, severe acute respiratory syndrome-coronavirus (SARS-CoV) and the Middle East respiratory syndrome (MERS), with the former being the more genetically similar to SARS-CoV-2; however, SARS-CoV-2 has proven to be even more contagious.[2,3,5]

Oxidative stress plays an underappreciated role in the COVID-19 infection,[9−17] with a recent study demonstrating that the age-dependent nature of its severity is linked to oxidative stress.[13] Cellular redox status is maintained by the thiol−disulfide balance that impacts viral fusion and entry processes.[11,18] Therefore, viral infections are presumably influenced by oxidative stress,[10,14,16−19] and COVID-19 disease is no exception. Studies found that disulfides, formed from the oxidation of cysteine thiols, are important for proper folding and conformational transition of the spike protein that facilitates viral entry into host cells.[20,21] Recently, the possibility of monitoring oxidative stress to study the spread

Received: September 17, 2021
Revised: November 8, 2021
Accepted: November 10, 2021

ACS Publications

© XXXX The Authors. Published by American Chemical Society

of COVID-19 has also been proposed[13] through an improved bioanalytical technique to determine the thiol−disulfide balance in the extracellular fluid.[22] As a result, a strategy of reducing oxidative stress was hypothesized,[15] and small molecule drugs with higher antioxidant potentials have been explored including N-acetyl cysteine, quercetin, l-ascorbic acid, and auranofin.[23−25] A recent study in a mouse model demonstrated that some of these drugs can prevent the infection and transmission of COVID-19.[21]

Although vaccination has been successfully employed in some economically affluent countries, the majority of the world is still under severe shortage of vaccine.[26] Additionally, the efficacy of the vaccine is under constant evaluation, especially as newer viral variants continue to emerge.[27−29] Therefore, a rigorous analysis of the cellular redox state and its impact on disease severity is long overdue. Using short simulations and neglecting differences due to entropic changes, our earlier study observed an increased binding affinity between the RBD of the S-protein and the peptidase domain (PD) of ACE2 under an oxidizing environment.[9] In the present study, we report a rigorous free-energy analysis using data from longer molecular dynamics (MD) simulations involving bound as well as individual protein partners. A detailed analysis of energetics, structural changes, and dynamics that aspires to unravel the interplay of oxidative stress and the binding affinity of the RBD to the extracellular PD of ACE2 is presented.

RESULTS AND DISCUSSION

Oxidative stress is the accumulation of reactive oxygen or nitrogen species (RONS) in the body such as peroxides, superoxide anion ($O_2^{\bullet-}$), and nitric oxide (NO).[16] Accumulation of these species impacts the thiol−disulfide equilibrium in the extracellular region and can alter the protein thiolation index.[13,22] There are seven disulfide linkages in the native SARS-CoV-2-bound ACE2 complex (PDB code: 6M0J[30]): four in the RBD of CoV-2 and three in the PD of ACE2 (Figure 1). In the present study, five different complexes of CoV-2 and ACE2 were constructed and studied: (i) the native complex CoV-2^{ox}···ACE2^{ox}, where all of the seven disulfide linkages (Figure 1) were retained; (ii) the CoV-2^{red}···ACE2^{ox} complex consisting of the RBD with four disulfides reduced to thiols and unaltered ACE2; (iii) a second CoV-2^{red-2}···ACE2^{ox}, where CoV-2 is reduced prior to binding; (iv) the CoV-2^{ox}···ACE2^{red} complex with the native RBD bound to the ACE2 with three disulfides reduced to thiols; and (v) CoV-2^{red}···ACE2^{red}, the complex where all of the seven disulfides were reduced to thiols. The protein partners were also simulated individually (unbound form) as a control: CoV-2^{ox} and ACE2^{ox} represent the RBD of CoV-2 and the extracellular PD of ACE2, respectively; the disulfides in both proteins were preserved. Similarly, CoV-2^{red} and ACE2^{red} represent the systems where all disulfides were converted to thiols. The effect of the reduction of these disulfides on the binding between the RBD of the S-protein and the PD of ACE2 was probed by studying interactions at the interprotein binding sites, energetics, collective dynamics, conformational changes, and per-residue fluctuations.

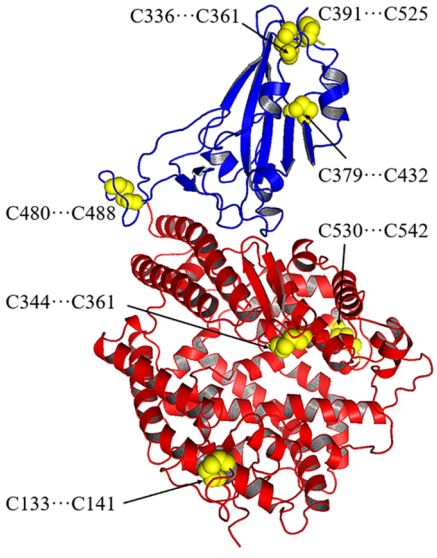

Figure 1. Location of the seven disulfide bonds in the RBD−ACE2 complex.

Interactions at the Protein−Protein Binding Interface

The binding interface of ACE2 and the RBD of the S-protein contains several interacting residues.[30,31] From the simulation data, these residues were studied by following the changes in their cumulative average of inter-residue distances and standard deviations as they evolved during the 200 ns of MD simulations (Tables S1−S4). Overall, three interacting zones were identified: left, central, and right (Figure 2). The left zone consists of a cluster of six residues (Table 1), contributed equally by both protein partners. The central zone is of similar size, consists of seven residues and contains a strong ion-pair interaction, K417(CoV-2)···D30(ACE2). The zone at the right is larger and consists of 11 residues (5 of CoV-2 and 6 of ACE2 subunits).

The reduction of the four disulfides of CoV-2 in the CoV-2^{red}···ACE2^{ox} complex impacted interactions present in the left and right zones. The interactions in the central zone remained intact, indicating that the overall interaction between the protein partners will remain strong upon the reduction of the CoV-2 disulfides (Table 1). The reduction of the three disulfides of ACE2 in CoV-2^{ox}···ACE2^{red} caused perceptible disruptions in the interactions on both left and right zones (Table 1). Much like the CoV-2^{red}···ACE2^{ox} system, interactions remained less affected in the central zone. However, the effect of reduction was most pronounced in the CoV-2^{red}···ACE2^{red} variant, where the interactions in the central zone were also impacted in addition to the left and right zones (Table 1).

The analysis of these interactions suggested that the central zone consisting of the α-helix (residues 19−53) of the ACE2 behaves as a hinge region. In particular, as observed in the collective motion analysis, the long helix acts like an axle on which the concave surface of the SARS-CoV-2 gets docked (*vide supra*). The interaction analysis revealed that the binding of the two proteins would be significantly impacted for the loss of all disulfide linkages, i.e., when all of the seven disulfides are reduced to thiols.

Energetics

In all cases, the overall binding was the result of favorable enthalpic changes offset by the unfavorable entropic penalty (Table 2). In other words, the combination of RBD−ACE2 interactions and the desolvation contributed to a net negative quantity of energy, whereas positive contributions resulted as the disorder of the entire system reduced upon binding (Table 2). Analysis of the native complex reveals that the

https://doi.org/10.1021/acsbiomedchemau.1c00040
ACS Bio Med Chem Au XXXX, XXX, XXX−XXX

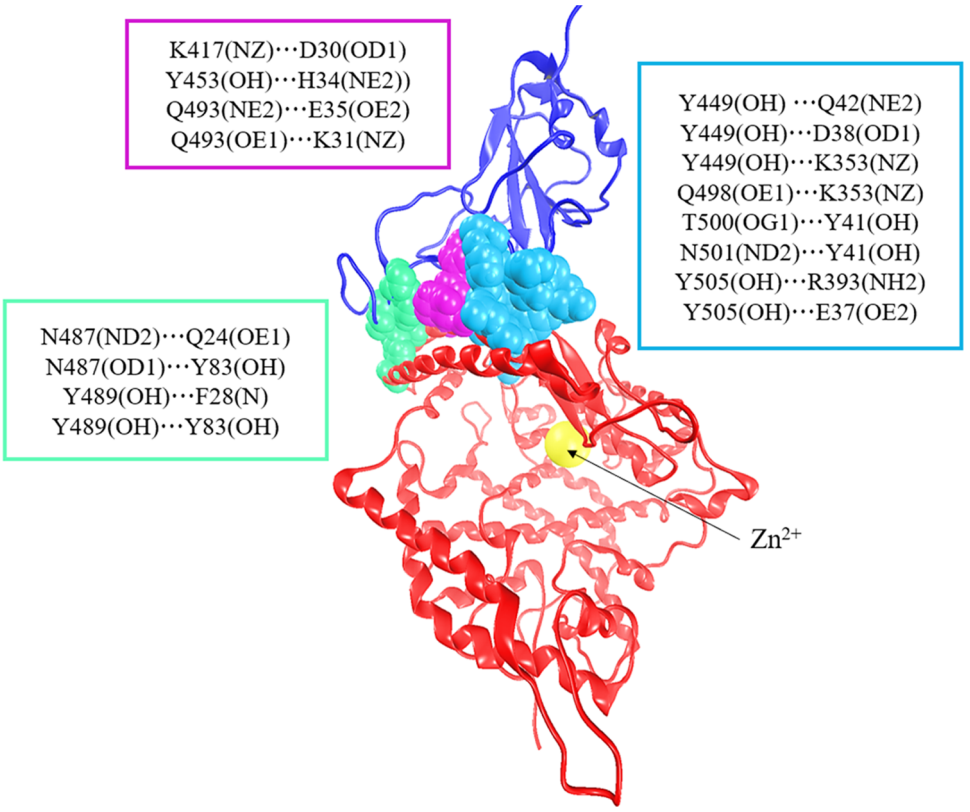

Figure 2. Three interaction zones in the SARS-CoV-2 RBD-bound ACE2: left (sea-green), central (purple), and right (cyan). The rectangular color-coded boxes display the interactions observed in this study. The central region contains the K417···D30 ion pair and other stronger interactions and acts like a hinge region. The ACE2 binds a Zn^{2+} ion at the catalytic pocket.

Table 1. Various Interaction Distancess between Rein the Three Zones Identified for the Protein Complexes at Different Oxidation States[a]

protein systems/zones	inter-residue interactions	CoV-2^{ox}···$ACE2^{ox}$	CoV-2^{red}···$ACE2^{ox}$	CoV-2^{ox}···$ACE2^{red}$	CoV-2^{red}···$ACE2^{red}$
left	Y489(OH)···F28(N)	4.4 (0.7)	4.8 (0.8)	4.2 (0.6)	5.6 (1.4)
	N487(ND2)···Q24(OE1)	5.3 (1.6)	7.7 (2.8)	6.9 (2.7)	11.3 (2.4)
	N487(OD1)···Y83(OH)	4.1 (1.4)	7.3 (2.3)	6.9 (2.3)	11.6 (2.6)
	Y489(OH)···Y83(OH)	4.2 (0.7)	4.6 (1.2)	4.7 (0.8)	7.6 (1.9)
central	K417(NZ)···D30(OD1)	4.7 (2.2)	5.3 (2.5)	5.4 (2.2)	4.0 (1.7)
	Y453(OH)···H34(NE2)	4.1 (0.7)	4.2 (0.7)	3.9 (0.7)	4.9 (1.7)
	Q493(OE1)···K31(NZ)	3.3 (0.9)	5.9 (2.8)	4.7 (2.2)	8.8 (1.8)
	Q493(NE2)···E35(OE2)	3.8 (0.9)	5.5 (2.2)	4.8 (1.6)	8.7 (3.2)
right	Y449(OH)···Q42(NE2)	5.9 (1.7)	7.9 (3.3)	12.6 (7.9)	15.9 (6.4)
	Y449(OH)···D38(OD1)	4.1 (1.5)	5.8 (2.6)	9.2 (7.7)	11.5 (6.0)
	Y449(OH)···K353(NZ)	5.5 (1.3)	9.7 (5.4)	9.4 (7.3)	12.3 (5.4)
	Q498(OE1)···K353(NZ)	5.4 (2.1)	8.6 (5.9)	4.4 (2.0)	7.0 (1.6)
	T500(OG1)···Y41(OH)	3.2 (0.5)	6.4 (2.4)	3.3 (0.3)	7.6 (1.6)
	N501(ND2)···Y41(OH)	4.4 (1.4)	7.1 (2.3)	6.0 (0.7)	9.7 (1.4)
	Y505(OH)···R393(NH2)	3.6 (0.4)	4.9 (1.9)	9.8 (0.8)	4.0 (0.9)
	Y505(OH)···E37(OE2)	3.4 (0.8)	5.7 (1.6)	7.1 (1.1)	6.6 (1.0)

[a]The inter-residue distances (in Å) are averaged over 200 ns of MD simulation with the standard deviation given in parenthesis.

contributions in terms of enthalpy and entropy were moderate with −33.2 and +22.8 kcal/mol, respectively (Table 2). For all other complexes, the entropic penalties were sharply higher in the range of 48−62 kcal/mol. The enthalpic changes due to binding became less favorable when either ACE2 or both protein partners were reduced to thiols (Table 2, column 2). The maximum loss of enthalpy was observed for the CoV-2^{red}···$ACE2^{red}$ complex, where all of the seven disulfides were converted to thiols. The decrease in enthalpic contribution corroborates with the structural incompatibility observed in the interaction analysis, as described earlier (Table 1 and Figure 2). Taken together, the Gibbs free energy of binding was impacted by the loss of the interactions at the protein−protein interface upon reduction of the disulfides to thiols.

For the native complex, the Gibbs free energy of binding is known and is equal to −10.4 kcal/mol.[4] Compared to the native, all systems exhibited decreased binding affinity with the reduction of disulfides (Table 2). The complex CoV-2^{red}···

https://doi.org/10.1021/acsbiomedchemau.1c00040
ACS Bio Med Chem Au XXXX, XXX, XXX−XXX

Table 2. Various Components (in kcal/mol) of the Gibbs' Free Energy of Binding of the RBD of SARS-CoV-2 to the PD of the ACE2 Receptor[a]

protein systems	total enthalpy $\Delta_{bind}H^{o}$ (*aq*)	entropic contribution $-T\Delta_{bind}S^{o}$ (*aq*)	Gibbs free energy $\Delta_{bind}G^{o}$ (*aq*)
CoV-2^{ox}···$ACE2^{ox}$	−33.2	22.8	−10.4[b]
CoV-2^{red}···$ACE2^{ox}$	−46.0 (−40.2)	48.7 (55.9)	2.7 (15.7)
CoV-2^{ox}···$ACE2^{red}$	−24.6	62.8	38.2
CoV-2^{red}···$ACE2^{red}$	−11.1	57.4	46.3

[a]The energy values in parentheses indicate the protein complex, where the RBD of CoV-2 was reduced prior to binding to the ACE2. [b]An experimental K_d value of −10.4 kcal/mol for the SAR-CoV-2···ACE2 complex, reported by Wang et al., was used as correction in eq 4.

$ACE2^{ox}$ exhibited a slightly positive binding affinity ($\Delta_{bind}G^{o}$ = 2.7 kcal/mol). The complexes CoV-2^{ox}···$ACE2^{red}$ and CoV-2^{red}···$ACE2^{red}$ exhibited large positive Gibbs' free energies of the binding with 38.2 and 46.3 kcal/mol, respectively.

Conformational Changes

To better understand the impact of oxidation on the conformation of the CoV-2···ACE2 complex, the root-mean-square deviation (RMSD) of the conformations of various complexes as they evolved during the 200 ns of MD simulations were analyzed (Figure 3a). In parallel, the study

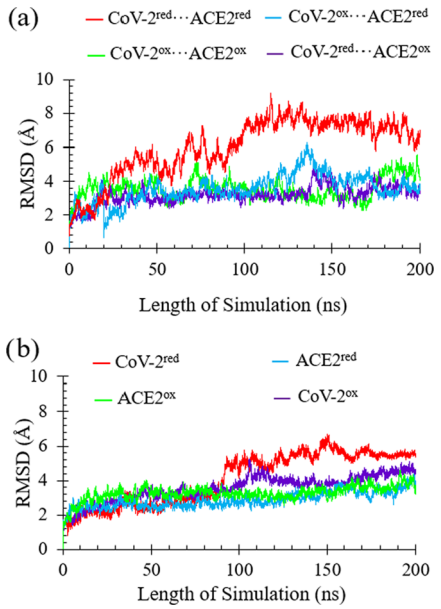

Figure 3. Root-mean-square deviation (RMSD) of the protein complexes of ACE2 and SARS-CoV-2 studied in this work. Disulfide variants (oxidized) are designated with a shorthand notation "ox", while thiol variants are denoted with a "red" notation.

was also extended to the unbound proteins, namely, CoV-2 and ACE2, in both oxidized and reduced states (Figure 3b). Beginning with the fully equilibrated protein conformations obtained through minimization, the RMSD of every conformation stored after each 10 ps interval was calculated. For a given system, the RMSD of each conformation was computed with respect to the reference structure obtained after minimization and was averaged over all C_α atoms (Figure 3a). In comparison to CoV-2^{ox}···$ACE2^{ox}$, neither the CoV-2^{red}···$ACE2^{ox}$ nor CoV-2^{ox}···$ACE2^{red}$ structures exhibited any significant RMSD from the reference structure across the 200 ns simulation. The trajectories for all three complexes exhibited fluctuations within 4 Å of their respective equilibrated starting conformations. However, the trajectory for the CoV-2^{red}···$ACE2^{red}$ complex (Figure 3a, red plot) exhibited significant deviation during the simulation. In particular, the fully reduced complex (CoV-2^{red}···$ACE2^{red}$) exhibited a large deformation (RMSD of ∼8 Å) from the starting structure, indicating a significant conformational change of the protein due to the reduction of all seven disulfide bonds.

As a comparative analysis of the conformational change, the RMSD from the initial structure for unbound protein partners was collected over the 200 ns of simulated dynamics (Figure 3b). For ACE2, the conformational change was insignificant for both the oxidized and the reduced states. As observed in Figure 3b, in both $ACE2^{ox}$ and $ACE2^{red}$ (green and cyan plots, respectively), the RMSDs were within 1.0 Å during the last 100 ns simulation. In contrast, the RBD of the CoV-2^{red} (Figure 3b, red plot) exhibited a sharp increase in the RMSD. Compared to the starting structure, the net change in RMSD was ∼5 Å. This observation illustrates a significant structural change occurring after 90 ns of simulations upon the reduction of disulfide bonds in the RBD of the S-protein. However, no significant conformational change was noted for the native RBD (CoV-2^{ox}; Figure 3b, purple plot).

The mode of binding of the two proteins suggests that the concave surface of CoV-2 binds over the two long helices (residues 19−53 and 55−84), which act like a hinge region (Figure 4a,b). As observed previously, the interactions in the central zone are stronger and help maintain the hinge motion observed during the simulated dynamics (Figure 4b). This is further established because the residue−residue interactions in the central zone and the hinge motion were maintained in all four protein−protein complexes.

Collective Protein Dynamics

In coordination with the analysis of RMSD, a study of essential dynamics[32,33] was performed to study the major displacements that occurred in the CoV-2···ACE2 complexes (Figure 5). As predicted, the principal motion of the native complex, CoV-2^{ox}···$ACE2^{ox}$, was found to exhibit an oscillatory motion in which the CoV-2 segment rotates over a hinge region on ACE2. Both CoV-2^{red}···$ACE2^{ox}$ and CoV-2^{ox}···$ACE2^{red}$ structures exhibited slight variations in their principal motions in comparison to CoV-2^{ox}···$ACE2^{ox}$. In all three complexes, the principal motion was represented by a rotation about the axis of the large ACE2 helix (res 19−53) anchored at the hinge region (Figure 4). In comparison to the initial structure, the final conformations in these three complexes were observed to be slightly distorted but consistent with the observed RMSD values (Figure 3). Similarly, the principal motion for the CoV^{red}···$ACE2^{red}$ complex significantly altered from that of the native CoV-2^{ox}···$ACE2^{ox}$ (Figure 5). Here, the CoV-2 segment seesawed over the interactive region, breaking all interactions in the hinge region (Figure 5). The final resting conformation dramatically varied from that of CoV-2^{ox}···$ACE2^{ox}$ and corroborates the significant divergence in the observed RMSD values.

https://doi.org/10.1021/acsbiomedchemau.1c00040
ACS Bio Med Chem Au XXXX, XXX, XXX−XXX

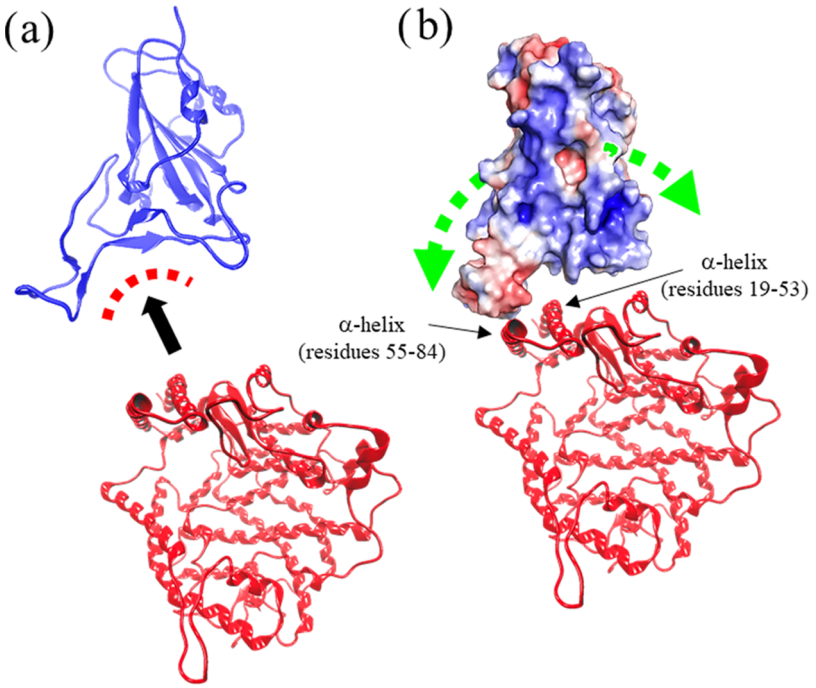

Figure 4. Oscillatory motion originates from the surface compatibility of the protein−protein binding interface.

Per-Residue Fluctuations

Using the 200 ns data for all protein systems, the root-mean-square fluctuations (RMSFs) were computed for each C_α atom. ΔRMSFs were calculated by subtracting the RMSFs of the native structure (CoV-2^{ox}···ACE2^{ox}) from the RMSF of the complex under consideration. Similarly, for ΔRMSFs of each individual protein partner, the oxidized forms (i.e., CoV-2^{ox} or ACE2^{ox}) were used as a reference. Therefore, the positive values of ΔRMSF indicate a higher backbone fluctuation of the region denoted by the residue number compared to the reference structure, as defined above. As illustrated in Figure 6a, significant backbone fluctuations were observed for the entire CoV-2 region when the disulfides of the RBD were reduced (CoV-2^{red}···ACE2^{ox} and CoV-2^{red}···ACE2^{red}). This is consistent with the significant displacement observed in the principal modes for these complexes (Figure 5). This is in contrast to the CoV-2^{ox}···ACE2^{red}, which exhibited only moderate changes in ΔRMSFs.

For the isolated ACE2 proteins (i.e. the reduced as well as the oxidized forms), the ΔRMSFs were insignificant for most residues (Figure 6b). However, for the reduced CoV-2 system, a major change was observed for the 470−505 residues, which is located at the binding interface forming the concave surface (Figure 6c, left). A longer (300 ns) MD simulation and conformational analysis of the CoV-2^{red} versus CoV-2^{ox} demonstrated that the conformational evolution (Figure S1) is consistent with the ΔRMSF analysis and corroborated that the reducing the disulfides of CoV-2 produces significant conformational changes of the binding motif. In particular, the loop (residues 470−505) was observed to undergo a major conformational change resulting in a complete loss of the concave surface, critical for the RBD of CoV-2 to bind the ACE2 (Figures 6c, right and 7).

Reduced RBD Prior to Binding

The effect of reducing the disulfides of the RBD prior to binding was also studied. The CoV-2^{red} conformation after 200 ns simulation was docked onto the binding site of ACE2 by superimposing the CoV-2^{red} backbone on the same unreduced RBD in the native complex. The complex was allowed to evolve through an additional 100 ns of molecular dynamics simulation. The structure exhibited significant differences in the interacting zone compared to those of the native complex due to the loss of structural compatibility (Figure S2). The computed free energy of binding was >15 kcal/mol (Table 2), which indeed demonstrates that the reduction of the RBD prior to binding will inevitably impair the binding (Figure 7). On the other hand, the oxidation of thiols to disulfides, known to be facilitated by oxidative stress,[34,35] appears to have produced a conformation of the RBD with much higher binding affinity for ACE2.

The present study did not measure the kinetics; however, using the thermodynamic results, one can assess the relative binding kinetics. Since the binding of oxidized protein partners (CoV-2^{ox}···ACE2^{ox}) is in the nanomolar range (15 nM),[8] the binding rate constant (k_{on}) is ∼10^7 times higher than the unbinding rate constant (k_{off}) as computed from the $\Delta_{bind}G^o$ (aq) value of −10.4 kcal/mol. If the reduction of disulfides of the CoV-2 RBD occurs before its binding with the ACE2, the k_{off} would be 10^{12} times higher than the binding rate constant ($\Delta_{bind}G^o$ (aq) = 15.7 kcal/mol). On the other hand, if the reduction occurs after the complex is formed, the k_{off} is increased only by 100-fold ($\Delta_{bind}G^o$ (aq) =2.7 kcal/mol). Therefore, it is likely that the timing of the reduction could have an impact on the viral protein binding to the cell surface receptors and subsequent fusion.

CONCLUSIONS

The redox dependency of the binding of the SARS-CoV-2 RBD with the human ACE2 receptor paints an unambiguous role of oxidative stress on the molecular basis of viral entry. Using 200 ns MD simulations, the interaction zone of the RBD−ACE2 complex and its evolved dynamics were studied for various oxidized (disulfide-containing) and reduced (thiol-

https://doi.org/10.1021/acsbiomedchemau.1c00040
ACS Bio Med Chem Au XXXX, XXX, XXX−XXX

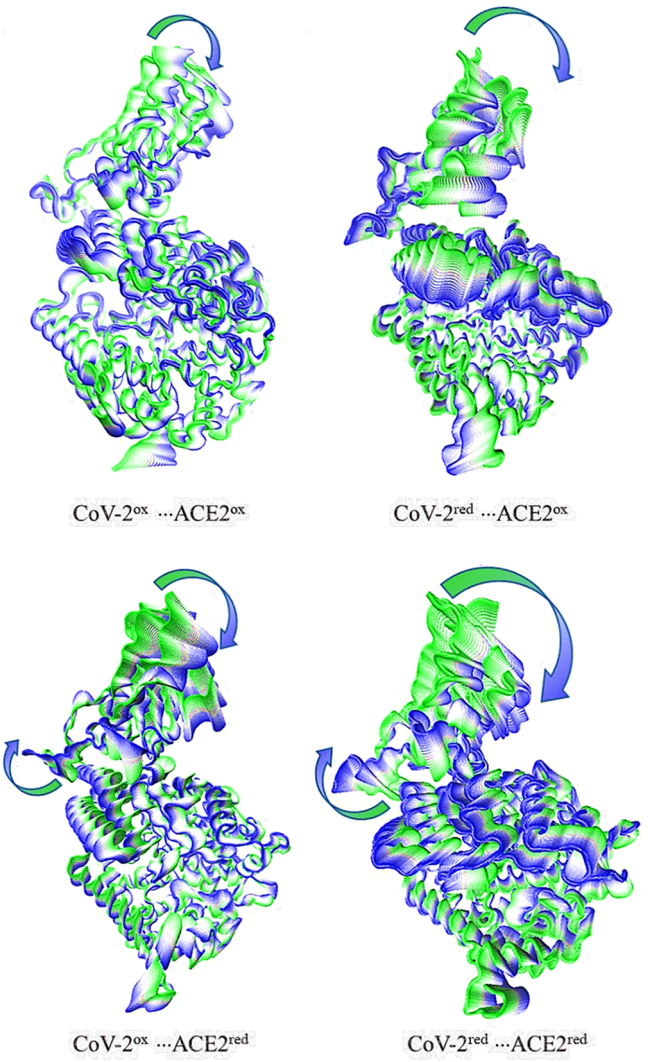

Figure 5. Oscillatory motion in the bound complexes observed from the essential dynamics analysis. The first principal component is shown for all of the protein complexes. The direction of conformational changes is shown using a color-coded scale with green (beginning) and blue (end).

containing) states of the RBD and ACE2. Free-energy calculations show that tighter binding in the native complex of SARS-CoV-2 RBD with ACE2 originates from a combination of enthalpic and entropic effects (Table 2). The study demonstrates that the disulfide-to-thiol conversion of CoV-2 and ACE2 impacts binding (Figure 7) and the binding completely perishes when either or both protein partners are reduced.

The most important finding of the present study is the significant impact of reduction on the binding affinity of the CoV-2 RBD to ACE2. Our study finds that when completely reduced prior to binding, a large conformational change occurs at the binding site of the CoV-2 (Figure 7). An assessment of binding free energy demonstrates that the binding is completely impaired with the host receptor as evident from a binding free energy of >15 kcal/mol. In other words, the oxidation of the RBD produced a conformation of the RBD that is ready to bind to the ACE2.

ACE2 can be found in the outer membrane of epithelial cells of various tissues including those of the lungs, heart, blood vessels, kidneys, liver, and gastrointestinal tract.[23−25] It plays an important role in regulating oxidative stress, acting as a catalyst for the conversion of angiotensin-II into the peptide, angiotensin 1−7 that acts to reverse the effects of angiotensin-II-related oxidative stress. Therefore, under normal conditions, ACE2 keeps oxidative stress in check. The binding of CoV-2 will inhibit the role of ACE2 in reducing oxidative stress and thus creating a vicious cycle, where the oxidative stress spirals out of control. Taken together, the study provides molecular-level insight into the mechanism by which oxidative stress plays a role in the COVID-19 infection. For the first time, the MD simulation study demonstrates that pre-existing oxidative stress creates a docking-ready conformation of the CoV-2 that has a significantly enhanced binding affinity toward human ACE2.

METHODOLOGY

Computational Setup

All protein complexes were prepared using visual molecular dynamics (VMD).[36] Disulfides were converted to thiols during this process using standard VMD scripting. All MD simulations were performed using GPU-enabled nanoscale molecular dynamics (NAMD)[37,38] alongside the CHARMM36 force field.[39,40] Electrostatic energy calculations during MD simulation were carried out using the particle mesh Ewald method.[41] Root-mean-square deviation (RMSD) calculations of the backbone carbon atoms were performed using VMD. Protein−protein interactions were analyzed using adaptive-basis Poisson−Boltzmann solver (APBS).[42] Electrostatic field calculations were performed using the PDB2PQR program suite.[43] Essential dynamics analysis and per-residue fluctuations were carried out using the program CARMA.[44]

MD Simulations

All simulations and analyses were conducted using the structure of human ACE2-bound SARS-CoV-2 (PDB entry: 6M0J).[30] For each set of simulations, the setup of protein complex systems was done using protocols established from previous studies.[38−41] Briefly, the HBUILD module of CHARMM was used to add hydrogens. Charges of acidic and basic amino acid residues were maintained corresponding to pH 7.0. The protonation state of histidine residues was determined through computation of the pK_a using the Propka option of PDB2PQR. The TIP3P model was used to solvate the protein systems alongside the addition of 24 sodium ions. The prepared protein complex systems were of dimensions 94 Å × 144 Å × 100 Å.

All protein complexes were subject to 50 ps minimizations. Following equilibrium, each system underwent 200 ns of MD simulation. Velocity Verlet integration algorithm was used to calculate atomic velocities and positions with a time step of 2.0 fs.[45] All MD simulations were run using NAMD implementation of Langevin dynamics under periodic boundary conditions and a constant temperature of 298 K.[38,39] Nonbonding interactions were modeled using a switching function with a "switchdist" of 10 Å, a cutoff of 14 Å, and a "pairlistdist" of 16 Å.

Binding Free-Energy Calculations

Gibbs free energies of binding for the protein−protein complexes were calculated using the adaptive Poisson−Boltzmann solver (APBS)[42] from their binding enthalpies and entropies

https://doi.org/10.1021/acsbiomedchemau.1c00040
ACS Bio Med Chem Au XXXX, XXX, XXX−XXX

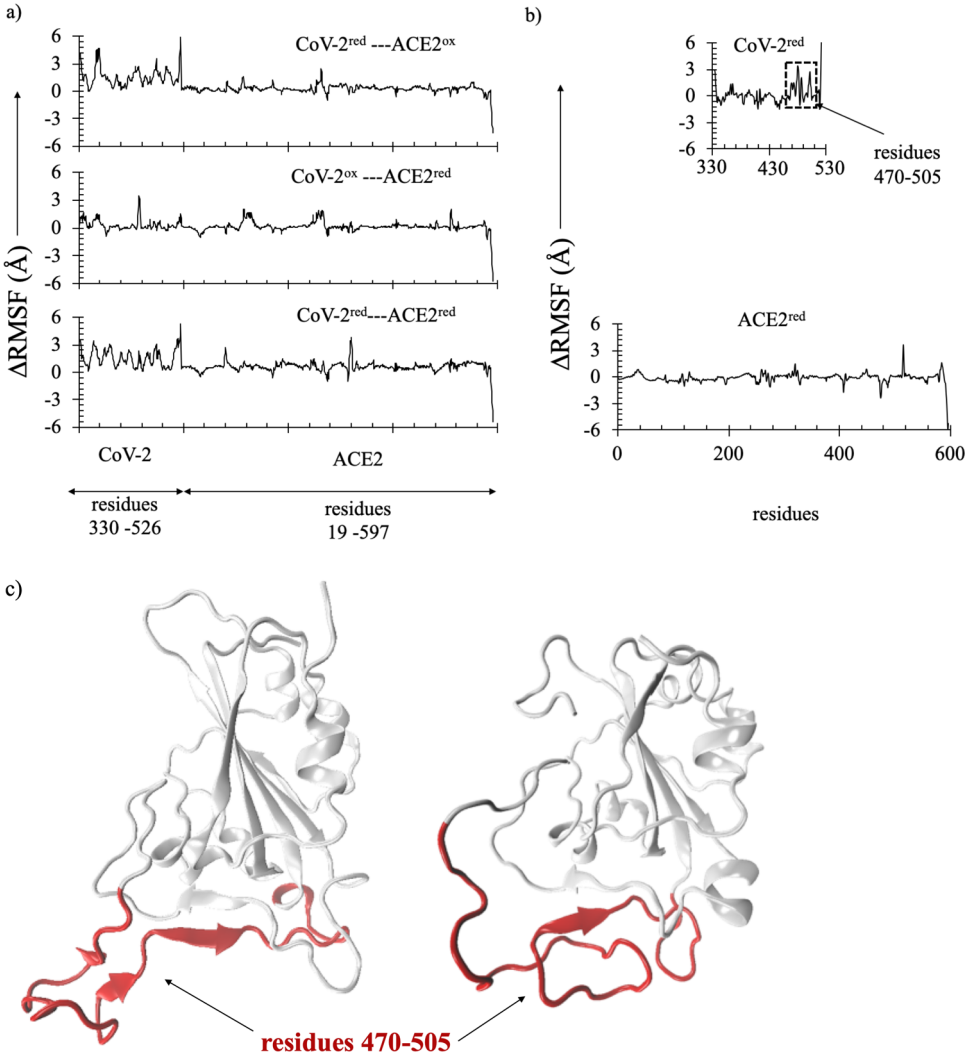

Figure 6. Conformational changes due to disulfide-to-thiol conversion: (a) difference in the per-residue fluctuations (ΔRMSF) in various thiol-containing reduced complexes with respect to the native state; (b) difference in the per-residue fluctuations (ΔRMSF) in the reduced monomer with respect to their corresponding oxidized state; and (c) the changed CoV-2 RBD conformation from the oxidized (left) to reduced (right).

$$\Delta_{\text{bind}}G_{\text{TABI-PB}} = \Delta_{\text{bind}}H_{\text{TABI-PB}} - T\Delta_{\text{bind}}S_{\text{TABI-PB}} \quad (1)$$

The $\Delta_{\text{bind}}H_{\text{TABI-PB}}$ was computed using the standard method of treecode-accelerated boundary integral Poisson−Boltzmann equation solver (TABI-PB)[46] within the APBS suite. Using this method, the protein surface was triangulated, and electrostatic surface potentials were computed. These discretized surface potentials were then used to calculate solvation energy and electrostatic (Coulombic) interactions among protein partners, as outlined in the thermodynamic scheme (Scheme 1)

$$\Delta_{\text{bind}}H_{\text{TABI-PB}} = \Delta_{\text{Coul}}H + \Delta\Delta_{\text{solv}}H \quad (2)$$

where $\Delta_{\text{Coul}}H$ represents the Coulombic interactions occurring at the protein−protein interface and $\Delta\Delta_{\text{solv}}H$ represents the difference in solvation energies between protein complexes and the respective free proteins (Scheme 1). The entropy part ($-T\Delta_{\text{bind}}S_{\text{TABI-PB}}$) in eq 1 was calculated following the standardized method described in Sun et al.[47] In this method, the interaction entropy of the protein−protein interactions was computed from the fluctuation of interaction energies. The interaction energies that fall within 3 times the standard deviation were used for the computation.[47] Since the calculated entropy change was based on the fluctuation of energies of the solvated enzyme system, the entropic change has been assumed to be the standard entropic change in the aqueous state

$$-T\Delta_{\text{bind}}S_{\text{TABI-PB}} = -T\Delta_{\text{bind}}S^{\circ}(aq) \quad (3)$$

Due to incomplete representation of the entire spike protein as well as ACE2, the experimentally known binding free energy of ACE2···CoV-2 was used to calibrate $\Delta_{\text{bind}}H_{\text{TABI-PB}}$ by ultimately correcting $\Delta\Delta_{\text{solv}}H$

$$\Delta E_{\text{corr}} = \text{RT ln } K_{\text{d}}(\text{CoV}{-}2^{\text{ox}}\cdots\text{ACE2}^{\text{ox}}) - \Delta_{\text{bind}}G_{\text{TABI-PB}}(\text{CoV}{-}2^{\text{ox}}\cdots\text{ACE2}^{\text{ox}}) \quad (4)$$

where K_{d} is the experimental dissociation constant, which is 37 nM.[48]

Therefore, the corrected free energy of solvation is

$$\Delta\Delta_{\text{solv}}H^{(\text{corr})} = \Delta\Delta_{\text{solv}}H + \Delta E_{\text{corr}} \quad (5)$$

The standard enthalpy of binding therefore can be obtained from eq 2 by replacing $\Delta\Delta_{\text{solv}}H$ with $\Delta\Delta_{\text{solv}}H^{(\text{corr})}$

$$\Delta_{\text{bind}}H^{\circ}(aq) = \Delta_{\text{Coul}}H + \Delta\Delta_{\text{solv}}H^{(\text{corr})} \quad (6)$$

https://doi.org/10.1021/acsbiomedchemau.1c00040
ACS Bio Med Chem Au XXXX, XXX, XXX−XXX

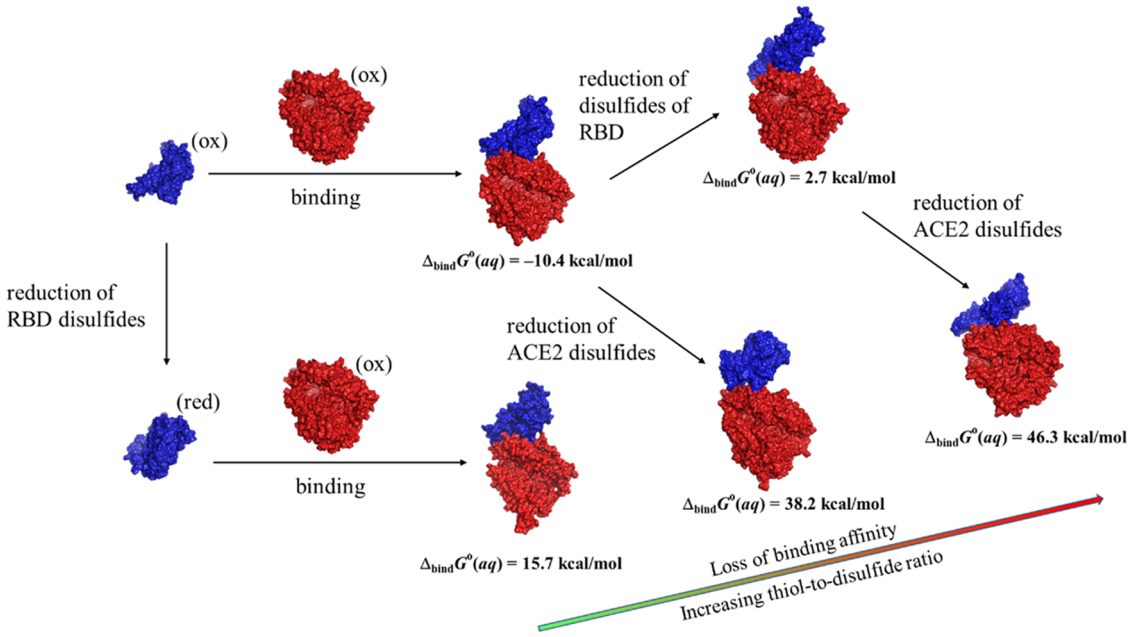

Figure 7. Conformational changes during a 200 ns MD simulation observed for the disulfide-reduced RBD domain of SARS-CoV-2 (blue color) in the free state versus bound to the PD of ACE2 (red color).

Scheme 1. Thermodynamic Diagram for Computing the Enthalpic Change for the Binding of the RBD of CoV-2 to the PD of ACE2

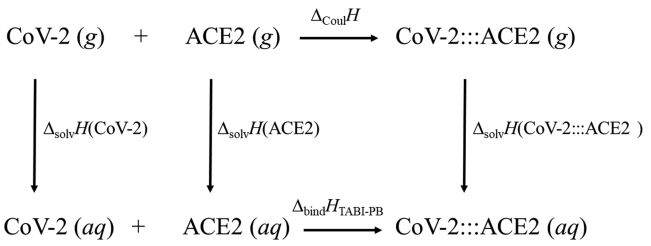

Using eqs 3 and 6, the aqueous binding free energy of the complex was computed by

$$\Delta_{bind}G^{o}\,(aq) = \Delta_{bind}H^{o}\,(aq) - T\Delta_{bind}S^{o}\,(aq) \quad (7)$$

■ ASSOCIATED CONTENT

Supporting Information

The Supporting Information is available free of charge at https://pubs.acs.org/doi/10.1021/acsbiomedchemau.1c00040.

Interaction distances of residues at the binding interface and figures depicting conformational changes of the SARS-CoV-2 RBD (PDF)

■ AUTHOR INFORMATION

Corresponding Authors

Sanchita Hati − *Department of Chemistry and Biochemistry, University of Wisconsin, Eau Claire, Wisconsin 54701, United States*; Phone: 715-836-2278; Email: hatis@uwec.edu

Sudeep Bhattacharyya − *Department of Chemistry and Biochemistry, University of Wisconsin, Eau Claire, Wisconsin 54701, United States*; orcid.org/0000-0002-3960-1239; Phone: 715-836-3850; Email: bhattas@uwec.edu; Fax: 715-836-4979

Authors

Carl J. Fossum − *Department of Chemistry and Biochemistry, University of Wisconsin, Eau Claire, Wisconsin 54701, United States*

Bethany F. Laatsch − *Department of Chemistry and Biochemistry, University of Wisconsin, Eau Claire, Wisconsin 54701, United States*

Harrison R. Lowater − *Department of Chemistry and Biochemistry, University of Wisconsin, Eau Claire, Wisconsin 54701, United States*

Alex W. Narkiewicz-Jodko − *Department of Chemistry and Biochemistry, University of Wisconsin, Eau Claire, Wisconsin 54701, United States*

Leo Lonzarich − *Department of Chemistry and Biochemistry, University of Wisconsin, Eau Claire, Wisconsin 54701, United States*

Complete contact information is available at: https://pubs.acs.org/10.1021/acsbiomedchemau.1c00040

Notes

The authors declare no competing financial interest.

■ ACKNOWLEDGMENTS

This work was supported, in part, by the National Institute of Health (grant number 1R15GM117510-01 to S.H. and S.B.). The computational resources of the study were provided by the Blugold Center for High Performance Computing under NSF grant CNS 1920220.

■ ABBREVIATIONS

ACE	angiotensin-converting enzyme
CoV	coronavirus
MERS	Middle East respiratory syndrome
MD	molecular dynamics

PD	peptidase domain
PDB	protein data bank
RBD	receptor-binding domain
SARS	severe acute respiratory syndrome
TABI-PB	treecode-accelerated boundary integral Poisson−Boltzmann

REFERENCES

(1) Arya, R.; Kumari, S.; Pandey, B.; Mistry, H.; Bihani, S. C.; Das, A.; Prashar, V.; Gupta, G. D.; Panicker, L.; Kumar, M. Structural Insights into SARS-CoV-2 Proteins. *J. Mol. Biol.* **2021**, *433*, No. 166725.

(2) Schoeman, D.; Fielding, B. C. Coronavirus Envelope Protein: Current Knowledge. *Virol. J.* **2019**, *16*, No. 69.

(3) Maier, H. J.; Bickerton, E.; Britton, P. Coronaviruses: Methods and Protocols; 2015; Vol. *1282*.

(4) Mittal, A.; Manjunath, K.; Ranjan, R. K.; Kaushik, S.; Kumar, S.; Verma, V. COVID-19 Pandemic: Insights into Structure, Function, and HACE2 Receptor Recognition by SARS-CoV-2. *PLoS Pathog.* **2020**, *16*, No. e1008762.

(5) Cui, J.; Li, F.; Shi, Z. L. Origin and Evolution of Pathogenic Coronaviruses. *Nat. Rev. Microbiol.* **2019**, *17*, 181−192.

(6) Wang, Y.; Liu, M.; Gao, J. Enhanced Receptor Binding of SARS-CoV-2 through Networks of Hydrogen-Bonding and Hydrophobic Interactions. *Proc. Natl. Acad. Sci. U.S.A.* **2020**, *117*, 13967−13974.

(7) Belouzard, S.; Millet, J. K.; Licitra, B. N.; Whittaker, G. R. Mechanisms of Coronavirus Cell Entry Mediated by the Viral Spike Protein. *Viruses* **2012**, *4*, 1011−1033.

(8) Wrapp, D.; Wang, N.; Corbett, K. S.; Goldsmith, J. A.; Hsieh, C. L.; Abiona, O.; Graham, B. S.; McLellan, J. S. Cryo-EM Structure of the 2019-NCoV Spike in the Prefusion Conformation. *Science* **2020**, *367*, 1260−1263.

(9) Hati, S.; Bhattacharyya, S. Impact of Thiol-Disulfide Balance on the Binding of Covid-19 Spike Protein with Angiotensin-Converting Enzyme 2 Receptor. *ACS Omega* **2020**, *5*, 16292−16298.

(10) Cecchini, R.; Cecchini, A. L. SARS-CoV-2 Infection Pathogenesis Is Related to Oxidative Stress as a Response to Aggression. *Med. Hypotheses* **2020**, *143*, No. 110102.

(11) Fenouillet, E.; Barbouche, R.; Jones, I. M. Cell Entry by Enveloped Viruses: Redox Considerations for HIV and SARS-Coronavirus. *Antioxid. Redox Signaling* **2007**, *9*, 1009−1034.

(12) Delgado-roche, L.; Mesta, F. Oxidative Stress as Key Player in Severe Acute Respiratory Syndrome Coronavirus (SARS-CoV) Infection. *Arch. Med. Res.* **2020**, *51*, 384−387.

(13) Giustarini, D.; Santucci, A.; Bartolini, D.; Galli, F.; Rossi, R. The Age-Dependent Decline of the Extracellular Thiol-Disulfide Balance and Its Role in SARS-CoV-2 Infection. *Redox Biol.* **2021**, *41*, No. 101902.

(14) Keles, E. S. Mild SARS-CoV-2 Infections in Children Might Be Based on Evolutionary Biology and Linked with Host Reactive Oxidative Stress and Antioxidant Capabilities. *New Microbes New Infect.* **2020**, *36*, No. 100723.

(15) Fratta Pasini, A. M.; Stranieri, C.; Cominacini, L.; Mozzini, C. Potential Role of Antioxidant and Anti-inflammatory Therapies to Prevent Severe SARS-CoV-2 Complications. *Antioxidants* **2021**, *10*, No. 272.

(16) Suhail, S.; Zajac, J.; Fossum, C.; Lowater, H.; McCracken, C.; Severson, N.; Laatsch, B.; Narkiewicz-Jodko, A.; Johnson, B.; Liebau, J.; Bhattacharyya, S.; Hati, S. Role of Oxidative Stress on SARS-CoV (SARS) and SARS-CoV-2 (COVID-19) Infection: A Review. *Protein J.* **2020**, *39*, 644−656.

(17) Paul, B. D.; Lemle, M. D.; Komaroff, A. L.; Snyder, S. H. Redox Imbalance Links COVID-19 and Myalgic Encephalomyelitis/Chronic Fatigue Syndrome. *Proc. Natl. Acad. Sci. U.S.A.* **2021**, *118*, No. e2024358118.

(18) Mathys, L.; Balzarini, J. The Role of Cellular Oxidoreductases in Viral Entry and Virus Infection-Associated Oxidative Stress: Potential Therapeutic Applications. *Expert Opin. Ther. Targets* **2016**, *20*, 123−143.

(19) Schwarz, K. B. Oxidative Stress during Viral Infection: A Review. *Free Radical Biol. Med.* **1996**, *21*, 641−649.

(20) Meirson, T.; Bomze, D.; Markel, G. Structural Basis of SARS-CoV-2 Spike Protein Induced by ACE2. *Bioinformatics* **2021**, *37*, 929−936.

(21) Manček-Keber, M.; Hafner-Bratkovič, I.; Lainšček, D.; Benčina, M.; Govednik, T.; Orehek, S.; Plaper, T.; Jazbec, V.; Bergant, V.; Grass, V.; Pichlmair, A.; Jerala, R. Disruption of Disulfides within RBD of SARS-CoV-2 Spike Protein Prevents Fusion and Represents a Target for Viral Entry Inhibition by Registered Drugs. *FASEB J.* **2021**, *35*, No. e21651.

(22) Giustarini, D.; Dalle-Donne, I.; Colombo, G.; Milzani, A.; Santucci, A.; Rossi, R. Protein Thiolation Index in Microvolumes of Plasma. *Anal. Biochem.* **2021**, *618*, No. 114125.

(23) De Flora, S.; Balansky, R.; La Maestra, S. Rationale for the Use of N-Acetylcysteine in Both Prevention and Adjuvant Therapy of COVID-19. *FASEB J.* **2020**, *34*, 13185−13193.

(24) Akhter, J.; Quéromès, G.; Pillai, K.; Kepenekian, V.; Badar, S.; Mekkawy, A. H.; Frobert, E.; Valle, S. J.; Morris, D. L. The Combination of Bromelain and Acetylcysteine (Bromac) Synergistically Inactivates Sars-Cov-2. *Viruses* **2021**, *13*, No. 425.

(25) Colunga Biancatelli, R. M. L.; Berrill, M.; Catravas, J. D.; Marik, P. E. Quercetin and Vitamin C: An Experimental, Synergistic Therapy for the Prevention and Treatment of SARS-CoV-2 Related Disease (COVID-19). *Front. Immunol.* **2020**, *11*, No. 1451.

(26) Forni, G.; Mantovani, A.; Forni, G.; Mantovani, A.; Moretta, L.; Rappuoli, R.; Rezza, G.; Bagnasco, A.; Barsacchi, G.; Bussolati, G.; Cacciari, M.; Cappuccinelli, P.; Cheli, E.; Guarini, R.; Bacci, M. L.; Mancini, M.; Marcuzzo, C.; Morrone, M. C.; Parisi, G.; Pasquino, G.; Patrono, C.; Curzio, A. Q.; Remuzzi, G.; Roncaglia, A.; Schiaffino, S.; Vineis, P. COVID-19 Vaccines: Where We Stand and Challenges Ahead. *Cell Death Differ.* **2021**, *28*, 626−639.

(27) Chakraborty, S. Evolutionary and Structural Analysis Elucidates Mutations on SARS-CoV2 Spike Protein with Altered Human ACE2 Binding Affinity. *Biochem. Biophys. Res. Commun.* **2021**, *534*, 374−380.

(28) Giovanetti, M.; Benedetti, F.; Campisi, G.; Ciccozzi, A.; Fabris, S.; Ceccarelli, G.; Tambone, V.; Caruso, A.; Angeletti, S.; Zella, D.; Ciccozzi, M. Evolution Patterns of SARS-CoV-2: Snapshot on Its Genome Variants. *Biochem. Biophys. Res. Commun.* **2021**, *538*, 88−91.

(29) Wadman, M. Israel's Grim Warning: Delta Can Overwhelm Shots. *Science* **2021**, *373*, 838−839.

(30) Lan, J.; Ge, J.; Yu, J.; Shan, S.; Zhou, H.; Fan, S.; Zhang, Q.; Shi, X.; Wang, Q.; Zhang, L.; Wang, X. Structure of the SARS-CoV-2 Spike Receptor-Binding Domain Bound to the ACE2 Receptor. *Nature* **2020**, *581*, 215−220.

(31) Ali, A.; Vijayan, R. Dynamics of the ACE2−SARS-CoV-2/SARS-CoV Spike Protein Interface Reveal Unique Mechanisms. *Sci. Rep.* **2020**, *10*, No. 14214.

(32) David, C. C.; Jacobs, D. J. Principal Component Analysis: A Method for Determining the Essential Dynamics of Proteins. *Methods Mol. Biol.* **2014**, *1084*, 193−226.

(33) Aalten, D. M. F. V.; Findlay, J. B. C.; Amadei, A.; Berendsen, H. J. C. Essential Dynamics of the Cellular Retinol-Binding Protein Evidence for Ligand-Induced Conformational Changes. *Protein Eng., Des. Sel.* **1995**, *8*, 1129−1135.

(34) Sevier, C. S.; Kaiser, C. A. Formation and Transfer of Disulphide Bonds in Living Cells. *Nat. Rev. Mol. Cell Biol.* **2002**, *3*, 836−847.

(35) Cumming, R. C.; Andon, N. L.; Haynes, P. A.; Park, M.; Fischer, W. H.; Schubert, D. Protein Disulfide Bond Formation in the Cytoplasm during Oxidative Stress. *J. Biol. Chem.* **2004**, *279*, 21749−21758.

(36) Humphrey, W.; Dalke, A.; Schulten, K. VMD: Visual Molecular Dynamics. *J. Mol. Graphics* **1996**, *14*, 33−38.

(37) Phillips, J. C.; Braun, R.; Wang, W.; Gumbart, J.; Tajkhorshid, E.; Villa, E.; Chipot, C.; Skeel, R. D.; Kalé, L.; Schulten, K. Scalable

https://doi.org/10.1021/acsbiomedchemau.1c00040
ACS Bio Med Chem Au XXXX, XXX, XXX−XXX

Molecular Dynamics with NAMD. *J. Comput. Chem.* **2005**, *26*, 1781−1802.
(38) Phillips, J. C.; Hardy, D. J.; Maia, J. D. C.; Stone, J. E.; Ribeiro, J. V.; Bernardi, R. C.; Buch, R.; Fiorin, G.; Hénin, J.; Jiang, W.; McGreevy, R.; Melo, M. C. R.; Radak, B. K.; Skeel, R. D.; Singharoy, A.; Wang, Y.; Roux, B.; Aksimentiev, A.; Luthey-Schulten, Z.; Kalé, L. V.; Schulten, K.; Chipot, C.; Tajkhorshid, E. Scalable Molecular Dynamics on CPU and GPU Architectures with NAMD. *J. Chem. Phys.* **2020**, *153*, No. 044130.
(39) Brooks, B. R.; Bruccoleri, R. E.; Olafson, B. D.; States, D. J.; Swaminathan, S. J.; Karplus, M. CHARMM: A Program for Macromolecular Energy, Minimization, and Dynamics Calculations. *J. Comput. Chem.* **1983**, *4*, 187−217.
(40) Brooks, B. R.; Brooks, C. L.; Mackerell, A. D.; Nilsson, L.; Petrella, R. J.; Roux, B.; Won, Y.; Archontis, G.; Bartels, C.; Boresch, S.; Caflisch, A.; Caves, L.; Cui, Q.; Dinner, A. R.; Feig, M.; Fischer, S.; Gao, J.; Hodoscek, M.; Im, W.; Kuczera, K.; Lazaridis, T.; Ma, J.; Ovchinnikov, V.; Paci, E.; Pastor, R. W.; Post, C. B.; Pu, J. Z.; Schaefer, M.; Tidor, B.; Venable, R. M.; Woodcock, H. L.; Wu, X.; Yang, W.; York, D. M.; Karplus, M. CHARMM: The Biomolecular Simulation Program. *J. Comput. Chem.* **2009**, *30*, 1545−1614.
(41) Essmann, U.; Lalith, P.; Berkowitz, M. L.; et al. A Smooth Particle Mesh Ewald Method. *J. Chem. Phys.* **1995**, *103*, 8577−8593.
(42) Jurrus, E.; Engel, D.; Star, K.; Monson, K.; Brandi, J.; Felberg, L. E.; Brookes, D. H.; Wilson, L.; Chen, J.; Liles, K.; Chun, M.; Li, P.; Gohara, D. W.; Dolinsky, T.; Konecny, R.; Koes, D. R.; Nielsen, J. E.; Head-Gordon, T.; Geng, W.; Krasny, R.; Wei, G. W.; Holst, M. J.; McCammon, J. A.; Baker, N. A. Improvements to the APBS Biomolecular Solvation Software Suite. *Protein Sci.* **2018**, *27*, 112−128.
(43) Dolinsky, T. J.; Nielsen, J. E.; McCammon, J. A.; Baker, N. A. PDB2PQR: An Automated Pipeline for the Setup of Poisson-Boltzmann Electrostatics Calculations. *Nucleic Acids Res.* **2004**, *32*, W665−W667.
(44) Glykos, N. M. Software News and Updates. Carma: A Molecular Dynamics Analysis Program. *J. Comput. Chem.* **2006**, *27*, 1765−1768.
(45) Verlet, L. Computer "Exyeriments" on Classical Fluids. I. Thermodynamical Properties of Lennard-Jones Molecules. *Phys. Rev.* **1967**, *159*, 98−103.
(46) Geng, W.; Krasny, R. A Treecode-Accelerated Boundary Integral Poisson-Boltzmann Solver for Electrostatics of Solvated Biomolecules. *J. Comput. Phys.* **2013**, *247*, 62−78.
(47) Sun, Z.; Yan, Y. N.; Yang, M.; Zhang, J. Z. H. Interaction Entropy for Protein-Protein Binding. *J. Chem. Phys.* **2017**, *146*, No. 124124.
(48) Yan, R.; Zhang, Y.; Li, Y.; Xia, L.; Guo, Y.; Zhou, Q. Structural Basis for the Recognition of SARS-CoV-2 by Full-Length Human ACE2. *Science* **2020**, *367*, 1444−1448.

https://doi.org/10.1021/acsbiomedchemau.1c00040
ACS Bio Med Chem Au XXXX, XXX, XXX−XXX